Simultaneous Force and Darkfield Measurements Reveal Solvent-Dependent Axial Control of Optically Trapped Gold Nanoparticles

Daniel J. Jackson[1], Brian A. Dawes[2], Maria Kamenetska[*1,2,3]

[1]Department of Chemistry, Boston University, Boston, MA 02215, United States.

[2]Department of Physics, Boston University, Boston, MA 02215, United States.

[3]Division of Material Science and Engineering; Boston University, Boston, MA 02215, United States.

Abstract

Single molecule force spectroscopy using optical tweezers (OT) has enabled nano-resolved measurements of dynamic biological processes but not of synthetic molecular mechanisms. Standard OT probes made from silica or polystyrene are incompatible with trapping in organic solvents for solution phase chemistry or with force-detected absorption spectroscopies. Here, we demonstrate optical trapping of gold nanoparticles in both aqueous and organic conditions using a custom OT and darkfield instrument which can uniquely measure force and scattering spectra of single gold nanoparticles (Au NPs) simultaneously. Our work reveals that standard models of trapping developed for aqueous conditions cannot account for the trends observed in different media here. We determine that higher pushing forces mitigate the increase in trapping force in higher index organic solvents and lead to axial displacement of the particle which can be controlled through trap intensity. This work develops a new model framework incorporating axial forces for understanding nanoparticle dynamics in an optical trap. These results establish the combined darkfield OT with Au NPs as an effective OT probe for single molecule and single particle spectroscopy experiments, with three-dimensional nanoscale control over NP location.

TOC graphic

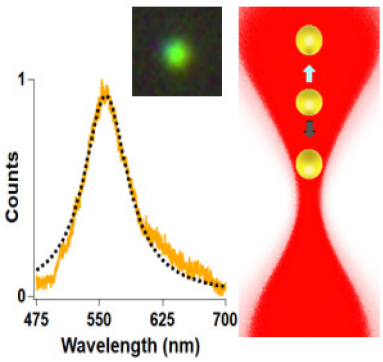

Optical tweezers (OT) have become an essential tool for mechanistic investigations of molecular processes in aqueous conditions,[1,2] providing insight into atomistic structure and energetics of biological machines and polymers. OT have higher force resolution of other force probes, such as the atomic force microscope (AFM), and function optimally in solution. The breakthroughs afforded by OT technology in biophysics and molecular biology were recognized by the 2018 Nobel Prize in Physics. Despite this demonstrated potential for studying single molecules and interactions, the OT technique has not been utilized in non-aqueous conditions to probe the structure, mechanics and energetics of non-biological polymers, molecular machines and solution-based chemistry. This gap is a result of incompatibility of most existing OT probes with organic solvent environments.[3–5] A lack of appropriate probes has also prevented OT from being applied to the growing field of chemical imaging using force-detected absorption spectroscopy, which has so far been almost exclusively performed with AFM at lower force resolution.[6–8] Here, we demonstrate optical trapping in common organic solvents using gold nanoparticles (Au NPs). We leverage our instrument's unique ability to trap, image and detect force of noble metal NP simultaneously to characterize, for the first time, and explain solvent-dependent trapping effects and dynamics of Au NP. We discover that modulating laser power can enable axial control of particle positions in organic solvents. Our work opens the possibility of in situ tracking of chemical transformations on the single molecule level using OT and of leveraging the unparalleled force resolution of the OT for force-detected absorption spectroscopy using plasmonics Au NPs.

The core of the OT instrument is an optical microscope combined with a laser beam focused at the sample plane. The beam focus applies a restoring force on dielectric microscopic particles and can confine them in 3-dimensions in solution. Commonly used dielectric probe materials, such as silica and polystyrene, are not suitable for tweezing in organic solvent environments or for force-detected absorption spectroscopies. A requirement for achieving stable trapping is a sufficient refractive index (RI) mismatch between the higher index dielectric particle and the lower index trapping medium.[9,10] Silica $(n_{silica} = 1.45)$ lacks the high RI mismatch with many organic solvents $\left(\text{typical } n_{organic} > 1.4\right)$. In contrast, a commonly used higher index material, polystyrene (PS) $(n_{PS} = 1.57)$, has a sufficient RI mismatch but breaks down in common organic solvents. Recent studies have used synthetic approaches to increase the effective RI of silica microspheres through the inclusion of a polystyrene or zinc oxide core.[3,4] However, these non-metallic probes are still not appropriate for force-detected spectroscopy where high polarizability is necessary.

An alternative trapping probe material for OT proposed here is a noble metal, such as gold or silver.[11] Gold nanoparticles (Au NP) have been shown to trap efficiently in water due to the high polarizability of metals.[12–15] The large magnitude of the dielectric constant of gold indicates that it will stably trap in the majority of available solvents. Gold is inert, but also functionalizable, in most solvent environments, and has the potential to serve as a universal OT

probe material in both aqueous and organic solvent conditions. Furthermore, trapping of highly polarizable metal NP has applications in force-detected absorption spectroscopies.[6–8,16,17] However, only *nano*scale Au particles less than ~200 nm in diameter can be stably trapped using a 1064 nm trapping beam due to excessive scattering forces which grow with increasing particle size.[14] Using sub-diffraction sized Au NP for trapping in conventional OT systems is challenging because they are not visible under standard bright field illumination.[18] In most prior work, integrated darkfield spectroscopy allowed imaging of the NP, but blocked the trapping laser detection channel, preventing particle displacement and force measurements.

Here, we demonstrate an instrument which overcomes these difficulties by combining an OT with a custom darkfield (DF) microscope and spectrometer module. With the addition of DF, we detect the trapped Au NPs through their plasmonic scattering. Unlike virtually all other reported setups, ours can record NP displacements and DF spectra in parallel, allowing correlative force and DF spectroscopy measurements.[19] This unique capability allows us to not only confine NP, but also characterize their diffusion and trapping efficiency to compare across solvent environments. This study is the first to demonstrate stable optical trapping of single Au NPs in organic solvent conditions, including in dimethylformamide (DMF), a common organic solvent compatible with solution phase chemistry, and to characterize the heating and dynamics of single particles. Using these measurements, we expand existing understanding of solvent-dependent optical trapping which can be leveraged for new application of single molecule and single particle spectroscopies. We find that trapping in DMF, while stable, is not as efficient as expected from standard models of trapping force which predict most efficient trapping of Au NP in high RI solvents. In contrast, our measurements show that trapping stiffness, which characterizes trapping efficiency, is lowest for DMF compared to other solvents in the transverse direction, (*x* direction in Figure 1A), and highest in the axial direction (*z* direction). By combining measurements of trap stiffness with standard models of heating, trapping, and scattering, we demonstrate that forces pushing particles out of the trap, which also depend on the RI, determine trapping efficiency trends across solvents. Specifically, the balance between the trapping and the pushing forces establishes the equilibrium *z* bead position downstream of the trap focus. We show that in DMF, this trapping equilibrium is furthest from the focus when compared to other solvents, resulting in the weakest transverse trap potential. By adjusting power, we can control not only the transverse direction stiffness, but also the axial position of the trapped particle. Overall, this work establishes Au NPs as promising OT probes across multiple solvent conditions with applications in single molecule and single particle optical and force spectroscopy measurements of non-biological polymers and small molecules.

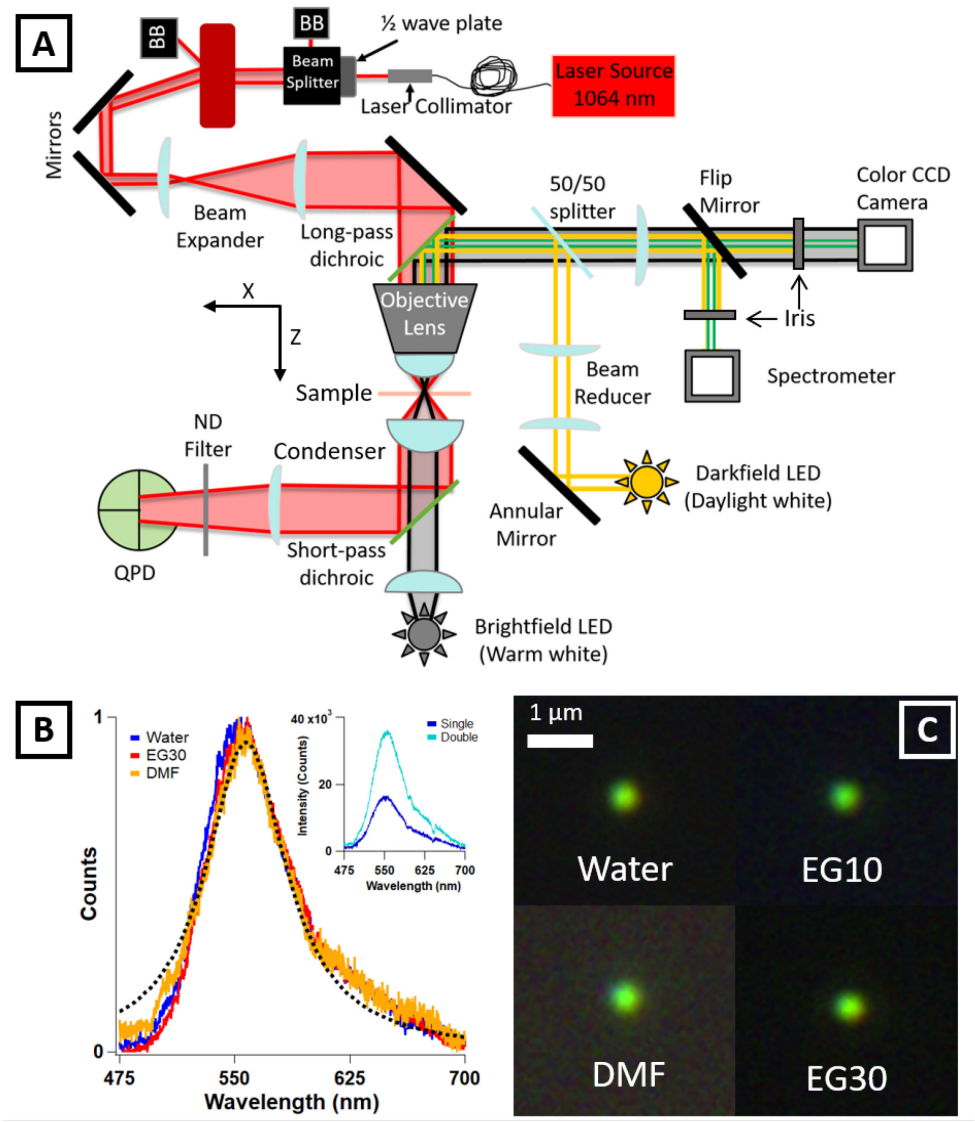

Figure 1. A) Instrument schematic of the custom built optical tweezer and DF microscope used here. B) LSPR scattering spectra of optically trapped 80 nm Au NP in a subset of solvents used here. Black dashed line is a Lorentzian fit for the DMF spectra. Inset: LSPR spectra of a single 80 nm Au NP (dark blue) and two 80 nm Au NP (pale blue) trapped in the OT. The peak in the spectrum shifts towards red and the intensity increases when two particles are trapped. C) DF images of 80 nm gold nanospheres trapped and suspended away from surfaces in different solvent environments. Spectra in (B) were recorded on the same particles as shown in images.

Figure 1A and S1 depicts our combined optical tweezer and DF microscope setup; details of the instrument are outlined in the SI. Briefly, we achieve stable OT using a collimated 1064 nm continuous wave Gaussian laser beam (IPG Photonics #YLR-5-1064-LP) which fills the back focal plane of the objective (Nikon #MRD01991) and is focused at the sample. We detect particle displacement in the trap using a standard back focal plane interferometry technique where the quadrant photodiode (QPD) (Mouser Electronics #718-QP154-QHVSD) images the back focal

plane of the condenser.[20] To enable DF, we use a white light emitting diode (LED) (Thorlabs #SOLIS-3C) and a custom annular mirror to generate a hollow, collimated, excitation beam expanded to fill the back of the trapping objective; this system replaces a standard DF condenser which blocks the trapping beam from the QPD. The scattered light from the Au NP is collected in an epi configuration by the same objective. An iris in the back focal plane acts ensures that only the scattered localized surface plasmon resonance (LSPR) signal is detected for analysis of trap contents.

Table 1: List of solvents used in this work and their relevant properties. Absorption cross sections are calculated for 1064 nm light and 80 nm Au NP, and then normalized compared to water. Cross section calculated using Equation S8.

Solvent	Viscosity at 25^{O}C (cP)	Refractive Index	Thermal Conductivity ($Wm^{-1}K^{-1}$)	Relative Absorption Cross-Sections
Water	0.91	1.33	0.606	1
10% Ethylene Glycol	1.03	1.34	0.565	1.024
30% Ethylene Glycol	1.72	1.36	0.488	1.075
50% Ethylene Glycol	3.00	1.38	0.420	1.128
Dimethylformamide	0.79	1.43	0.184	1.266

The strength of our combined OT and DF setup is that it allows simultaneous trapping, spectroscopic imaging and force sensing of the nanoparticles in various solvent and chemical environments. We use DF to see the Au NP in the far field in our microscope, which makes the trapping experiment possible. Additionally, we direct the collected DF signal into a spectrophotometer to detect the LSPR spectrum, which is highly sensitive to the particle size, shape, and material.[21,22] In parallel, we measure the particle diffusion and force using the QPD signal.

The solvents used in this work are listed in Table 1 along with their relevant physical properties. Water has the lowest RI of 1.33. We combine water and varying fractions of ethylene glycol (EG) to produce mixtures containing 10%, 30%, and 50% EG, denoted as EG10, EG30, and EG50 respectively. These mixtures are characterized by increasing RI values and decreasing thermal conductivity when compared to water. We also use DMF, which has the highest RI of 1.43 and by far the lowest thermal conductivity of solvents in our experiments.

Representative spectra and DF images of single Au NPs stably trapped in water, EG10, EG30 and dimethylformamide (DMF) are shown in Figure 1B and C respectively. In all solvents, we are able to catch an Au NP in the OT by tracking it in the DF, and collect a DF color image and LSPR spectra to differentiate single trapped particles from doubles or clumps (Figure 1B inset).

The spectra of single Au NPs in Figure 1B fit well to a single Lorentzian line shape, as shown with a dashed line for DMF. The fits reveal maximum scattering at 555-560 nm, which is consistent with predicted scattering of single spherical 80 nm Au particles (see SI for more details). Importantly, the presence of two or more particles within the trap results in higher LSPR intensity, red-shifted spectra, and distinct particle displacements as shown in the inset of Figure 1B and Figure S2.

Once a single Au NP is trapped and detected in the DF, we can track the position of the particles undergoing Brownian motion relative to the trap focus, which is defined as zero displacement.[23] We use an established calibration procedure to determine a conversion between QPD voltage signal and distance units.[20] The resulting NP displacements along the x direction indicated in Figure 1A, recorded at 400kHz over 3 seconds with a trapping laser power of 32 mW, are plotted as a time course and binned in a histogram in Figure 2A, left and right panels respectively. We observe that for all solvents, the particle displacements are normally distributed as expected for a quadratic confining potential, which indicates stable trapping in all solvents.[24] We note that Au NPs can remain dispersed in all solvents for days and even weeks without deteriorating, demonstrating true stability in both aqueous and organic conditions.[4]

We can now compare trapping efficiency of Au NPs across varying solvent conditions. According to standard models, it is expected that trapping of noble metal nanoparticles should be more efficient in organic solvents, which have a higher RI than water. The restoring trapping force, F_{grad}, is due to the gradient of the electric field intensity, I, and scales with the particle polarizability, α, which depends on the dielectric constant mismatch:

$$F_{grad} = \frac{|\alpha|}{4} \nabla \mathrm{I} \,, \qquad \alpha = 3V_p \left(\frac{\varepsilon_p - \varepsilon_m}{\varepsilon_p + 2\varepsilon_m} \right)$$

Equation 1

In equation 1, ε_m is the medium dielectric constant, ε_p is the particle dielectric constant, and V_p is the particle volume (see the SI for more details).[9,12] Dielectric constant relates to RI by $n = \sqrt{\varepsilon}$. Based on equation 1, we expect trapping efficiencies at small displacements to scale linearly with trapping beam power for Gaussian beams as derived in equation S7 in the SI. Furthermore, we see that for particles with a large imaginary component of n_p, such as Au NPs, α and thereby F_{grad}, increase with n_m. Following this reasoning, we expect an increase in trapping stiffness with increasing solvent RI.

To characterize trapping efficiency experimentally, we use the measured displacements to construct PSDs of particle motion, as shown in Figure 2B. In all solvents, the PSD shows a characteristic Lorentzian shape, indicating stable trapping. We observe that both Lorentzian fit parameters—the cut-off frequency, f_c, and the amplitude A—depend on the solvent environment. Specifically, f_c is greatest for DMF and least for EG50, while *A* shows the reverse

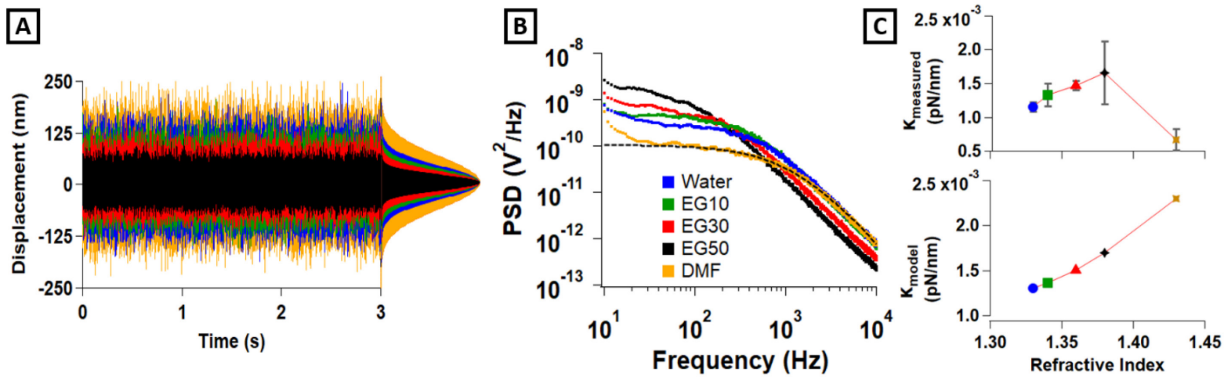

Figure 2. A) Displacements of 80 nm Au NP trapped in the OT (left) and displacement histograms (right) in various solvents. Slow drift has been subtracted from the data. B) PSD of optically trapped 80 nm Au NPs in different solvents determined from displacements in Figure 1D. PSD curves have been smoothed to 10 Hz. Dashed line shows a Lorentzian fit to the DMF data. C) Top plot shows the measured stiffness at 32 mW based against refractive index of the medium. Bottom plot is modelled stiffness at 32 mW of 80 nm Au NP using equation 1.

trend. Both of these parameters reflect the varying solvent conditions, such as viscosity and heating in the trap, as well as potentially real changes to trapping efficiency, characterized by stiffness, in the various media.[20] Stiffness κ is related to f_c through

$$\kappa = 12\pi f_c \eta R$$

Equation 2

Here η is the viscosity of the solvent and *R* is the particle radius. The Lorentzian amplitude *A* can be related to the diffusion constant, *D*, of the particle in each solvent.[20] According to Einstein's diffusion equation, D is related to solvent viscosity η through

$$D = \frac{k_B T}{6\pi\eta R}$$

Equation 3

We note that the viscosities, η, of the solvents in this study, listed in Table 1, vary by a factor of three. Thus, we cannot related measured differences in f_c between solvents directly to stiffness values using equation 2 as is often done for aqueous conditions. Furthermore, gold absorbs the 1064 nm trapping laser illumination, leading to significant heating around the trapped particle.[25] The expected surface temperatures of Au NP under 1064 nm illumination in different solvents are calculated in the SI. The temperature increase in organic solvents like DMF is expected to be higher than in aqueous conditions due to higher particle polarizability in high RI media and lower thermal conductivity, leading to a further divergence of their viscosity values.

We account for these differences in solvent environments and for heating effects by determining *D* directly from our measurements and extrapolating η using equation 3 before solving for stiffness.[25] First, we use a heating model, detailed in the SI, to calculate the temperature in the immediate vicinity of the trapped particles. The model accounts for the absorption cross section of Au NPs in various solvents, the power density of the laser at the

trapping point as shown in Figure S3 and equations S1 and S2, and the thermal conductivity of the solvent. This model has been previously shown to accurately predict temperature around Au NP in water (see SI for full model description).[12,25] The calculated temperature values are shown in Figure S4.

Next, we measure the diffusion constant value *D* from the *A* fit parameter and input the calculated temperature from Figure S4 into equation 3 to calculate a viscosity which is input into equation 2 to determine the stiffness.[20] For each power setting and solvent, we average viscosity and stiffness values determined from at least 10 different Au NPs with a recorded displacement trajectory lasting at least 20 seconds. We note that the resulting viscosities plotted in Figure S5 match the expected viscosity at the calculated temperatures, confirming that our results are self-consistent and properly account for heating effects.

The average stiffness values determined at 32 mW trapping laser power are plotted against the RI of the solvent in Figure 2C (top) and compared to the model stiffness predictions (bottom). We observe the expected increase in trapping efficiency with RI for water and EG mixtures. Surprisingly, we find that DMF has the lowest stiffness of the solvents in our sample, contradicting the model prediction in equation 1.

Figure 3A shows the effect of increasing laser intensity on stiffness in all solvents. We observe that in water and EG10, the increase in trapping efficiency is linear, in agreement with equation 1 as detailed in the SI. In all other solvents we observe a significant deviation from expected linear behavior, particularly in EG50 and DMF.[25,26] We note that the deviation from linearity increases concomitantly with the increase in RI of the solvent and becomes more apparent at high trapping laser powers. In EG50 and DMF, there is a dramatic acceleration of stiffness increase just above and below 50 mW of power, respectively. Previously, such superlinear increases of stiffness with laser power have been attributed to unaccounted heating in the trap.[25] However, heating effects are fully corrected for in our measurements here as described above. Furthermore, in DMF where the temperature is highest (Figure S4), the stiffness becomes supralinear as power increases further. Notably, the stiffness observed in DMF remains below that of lower RI solvents at all powers.

Trapping along the laser propagation direction, z in Figure 1A, is expected to be less efficient due to the pushing forces the particle experiences from backscattering and absorption of laser light.[27] Yet the trapping stiffness along the z direction, κ_z, should also scale with RI according to Equation 1, with high RI solvents showing the most efficient trapping.[27] We measure κ_z values and compare to the trends in κ_x. We construct PSD spectra of particle z-displacements, fit a Lorentzian to extract the corner frequency and use equation 2 to determine the z-direction stiffness, with the diffusion constant, *D*, and temperature, *T*, determined as described above.

The resulting κ_z values are plotted in Figure 3B. We note that trapping efficiency in the z-direction is ~10-fold lower than in the x-direction. In both cases, the stiffness increases with increasing power. For κ_z, the trends in EG50 and DMF are superlinear and supralinear,

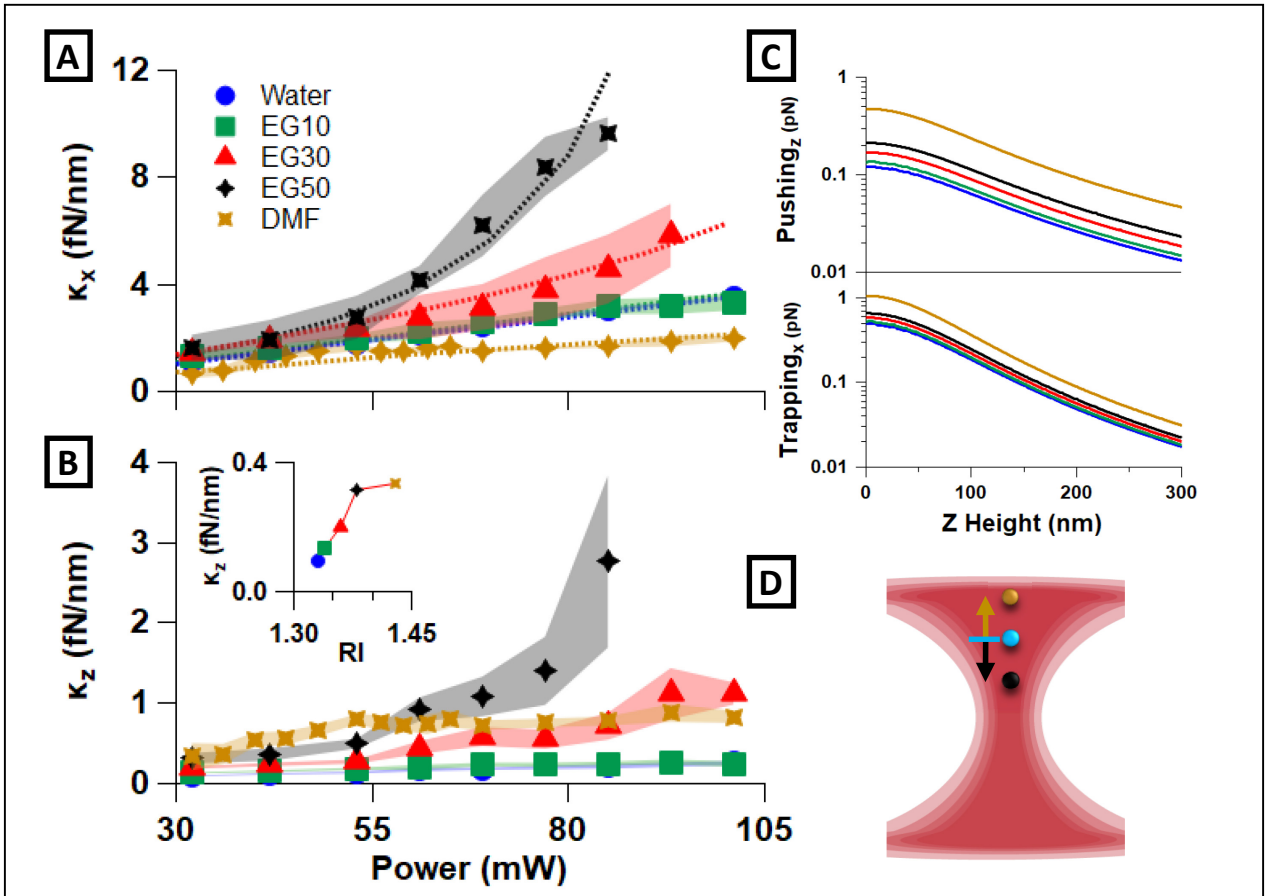

Figure 3. (A) Measured stiffness values in the x direction of an optically trapped, 80 nm gold nanoparticle in various solvents as a function of power. Dashed lines represent predicted stiffness based off models for trapping and pushing forces experienced by a particle in an optical trap. B) z direction stiffness values associated with x stiffness values from (A). Inset shows the trend of stiffness against refractive index at 32 mW trapping power C) Calculated trapping force in the transverse plane (top) and the scattering force in the axial direction (bottom). D) Cartoon illustration of particle equilibrium position in the axial direction in various solvents. In water (blue) the particle trapping position remains fixed regardless of power, while in EG50 (black) and DMF (brown) it is displaced towards and away from the focal point respectively.

respectively. Importantly, κ_z scales with RI according to equation 1 as is emphasized in the inset of Figure 3B which plots κ_z measured at 32 mW in all solvents. We observe that κ_z in DMF has the highest value, in contrast to the trend in κ_x.

These results affirm that trapping in high RI solvents like DMF can be more efficient, as predicted. However, many variables vary across solvent conditions and are not accounted for in equation 1. We already showed that varying temperature across solvents cannot explain the trends observed here. Another solvent dependent variable is the pushing force, which is the sum of the scattering and absorption forces on the particle in the trap. It increases with the RI of the medium as shown in equation S8. In water, it was previously reported that the equilibrium between the trapping and pushing forces results in the particle being trapped ~200 nm

downstream along the positive *z* axis from the laser focus.[25,28] We hypothesize that the balance of the trapping and pushing forces may be different depending on the solvent environment and the trapping power.

We calculate both the z-dependent axial pushing and the transverse trapping forces for 32 mW of power as detailed in the SI and plot them in Figure 3C, top and bottom respectively. We note that both forces decrease as the distance from the focus along the propagation direction, z, grows. At all z locations, both forces are greatest for DMF as expected. However, the difference between solvents is most pronounced in the pushing force, where DMF shows the highest value by a factor of at least 2. These results suggest that Au NP in DMF may be trapped further away from the laser focus than in lower RI solvents due to increased pushing. Consulting Figure 3C (bottom), we observe that a particle trapped in DMF at ~300 nm along the z direction would indeed trap more weekly than a particle in water at ~200 nm, in agreement with the trends measured in Figure 3A. As the power grows, the trapping and pushing forces increase at different rates, resulting in changes in the equilibrium trapping position.

To test these assumptions, we fit equation S7, which describes the z-dependence of the transverse trapping stiffness, to our measured κ_x data. Specifically, we use the z-distance as the fit parameter and allow it to change linearly with laser power. We adjust the proportionality constant between laser power and z-distance until good agreement between the model and our stiffness data is achieved at every power setting. The resulting calculated stiffness values are plotted in dashed lines alongside measurements in Figure 3A. We find excellent agreement of the model with our data for all solvents when z-value changes are incorporated. For water and EG10, no change in z-position is required to achieve a good fit to the data and z=200 nm at all powers as found previously.[25,28] As a result, the stiffness grows linearly with intensity. In contrast, in EG30 and EG50, we find that allowing the particles to move closer towards the focal plane with increasing power produces a superlinear trend matching our observations. Specifically, in EG30 and EG50, the best fit is obtained if the particles start at z=200nm and 210nm, shifting to lower z values at a rate of 0.2 nm/mW and 1 nm/mW, respectively. Finally, in DMF, the particle starts at z=275 nm and shifts *away* from the focus by 1 nm/mW, resulting in a supralinear dependence of stiffness on power, matching the trend in our measurements. We note that predictions fall inside the standard error (shaded regions) with minor exceptions at intermediate power for DMF.

The summary of these solvent-dependent effects is shown in the cartoon in Figure 3D. We find here that the equilibrium trapping position along the z-direction is a solvent-dependent parameter affecting measured stiffness in the transverse plane. In low RI solvents like water, Au NPs remain fixed at a near constant distance from the focus as the power increases (blue dot), resulting in a linear increase of stiffness with power. In medium RI solvents, the increase in the trapping dominates the increase in the pushing force, leading to a reduction in z and a superlinear increase of stiffness with power as the particle becomes more strongly trapped as a result of two simultaneous effects (black dot). Finally, in high RI solvents like DMF, the pushing overtakes the

trapping force and expels the particles further away from the focus where the beam is more diffuse and trapping is weaker (brown dot). This shift counteracts the effects of higher power on trapping and results in a plateauing of stiffness.

In conclusion, using a custom instrument with uniquely combined DF and OT capabilities, we characterize, for the first time, trapping trends of spherical Au NPs in a variety of dispersion media, including the organic solvent DMF, which is commonly used for solution phase chemistry. Our work lays the foundation for single molecule solution phase chemistry experiments and force-detected absorption spectroscopy using OT. We use DF spectroscopy to measure the LSPR fingerprint of individual NPs to determine, unambiguously, that we have trapped only a single NP in various solvents. We find that trap stiffness generally increases with increasing RI of the medium, as predicted by standard models of gradient forces on a dipole in an electric field, but deviates from this trend for DMF. We model the temperature of the solvent near the trapped NP to establish that the temperature increases rapidly with power in organic solvents, where the particle polarizability is high and thermal conductivity low. Nevertheless, these effects alone cannot account for the deviations from expected behavior in our stiffness data. Instead we find that pushing forces resulting from scattering and absorption of the laser light by the trapped NP scale with RI and power and may shift the equilibrium trapping location relative to the focus of the beam. Good agreement with the data is achieved in the model when we allow the particle axial trapping location to vary with solvent and with power in higher RI solvents. These results suggest that differences between solvents may have effects on particle behavior in OT that are not well explained by simple theories of trapping. We provide a more comprehensive model of trapping than previously used which incorporates both trapping and pushing forces to explain the observed trends. Future work is needed to test these proposals in a wider range of solvent conditions. Overall, our work suggests that Au NPs are effective optical trapping probes in a variety of conditions and opens the possibility of controlled heating and nanoscopic 3D manipulation of metallic NPs in organic solvents. The advances in instrument design and modeling we outline here establish foundations for single molecule force spectroscopy and force-detected absorption spectroscopy for solution phase chemistry experiments using optical trapping and Au NP.

ASSOCIATED CONTENT

Supporting Information

The following files are available free of charge: TrappingAuNPorganics_SI.pdf. This material contains additional figures and equations explaining the derivation of trapping, scattering forces and heating models.

AUTHOR INFORMATION

Corresponding Author

* Maria Kamenetska; orcid.org/0000-0002-0390-035X; Email: mkamenet@bu.edu

Author Contributions

The manuscript was written through contributions of all authors. All authors have given approval to the final version of the manuscript.

Funding Sources and acknowledgement

DJ acknowledges support from a BUnano Cross-Disciplinary Fellowship. All authors acknowledge support from the Boston University Photonics Center. MK acknowledges NSF award #2117585.

Bibliography

(1) Bustamante, C. J.; Chemla, Y. R.; Liu, S.; Wang, M. D. Optical Tweezers in Single-Molecule Biophysics. *Nat. Rev. Methods Prim. 2021 11* **2021**, *1* (1), 1–29. https://doi.org/10.1038/s43586-021-00021-6.

(2) Zaltron, A.; Merano, M.; Mistura, G.; Sada, C.; Seno, F. Optical Tweezers in Single-Molecule Experiments. *Eur. Phys. J. Plus* **2020**, *135*, 896. https://doi.org/10.1140/epjp/s13360-020-00907-6.

(3) Black, J. W.; Kamenetska, M.; Ganim, Z. An Optical Tweezers Platform for Single Molecule Force Spectroscopy in Organic Solvents. *Nano Lett.* **2017**, *17* (11), 6598–6605. https://doi.org/10.1021/acs.nanolett.7b02413.

(4) Yu, Q.; Chen, Y.-N.; Black, J. W.; Ganim, Z. Zinc Oxide @ Silica Core/Shell Microspheres for Single-Molecule Force Microscopy in Aqueous and Non-Aqueous Solvents. *J. Phys. Chem. C* **2020**, *124*, 5789–5795. https://doi.org/10.1021/acs.jpcc.9b11923.

(5) Yusof, M. F. M.; Ayop, S. K.; Supian, F. L.; Juahir, Y. Optical Trapping of Organic Solvents in the Form of Microdroplets in Water. *Chem. Phys. Lett.* **2020**, *749*, 137407. https://doi.org/10.1016/j.cplett.2020.137407.

(6) Nowak, D.; Morrison, W.; Wickramasinghe, H. K.; Jahng, J.; Potma, E.; Wan, L.; Ruiz, R.; Albrecht, T. R.; Schmidt, K.; Frommer, J.; et al. Nanoscale Chemical Imaging by Photoinduced Force Microscopy. *Sci. Adv.* **2016**. https://doi.org/10.1126/sciadv.1501571.

(7) O'callahan, B. T.; Yan, J.; Menges, F.; Muller, E. A.; Raschke, M. B. Photoinduced Tip−Sample Forces for Chemical Nanoimaging and Spectroscopy. *Nano Lett.* **2018**, 5499–5505. https://doi.org/10.1021/acs.nanolett.8b01899.

(8) Parobek, A.; Black, J. W.; Kamenetska, M.; Ganim, Z. Force-Detected Nanoscale Absorption Spectroscopy in Water at Room Temperature Using an Optical Trap. *J. Chem. Phys.* **2018**, *148* (14). https://doi.org/Artn 14420110.1063/1.5017853.

(9) Ashkin, A.; Dziedzic, J. M.; Bjorkholm, J. E.; Chu, S. Observation of a Single-Beam Gradient Force Optical Trap for Dielectric Particles. *Opt. Lett.* **1986**, *11* (5), 288–290.

(10) Neuman, K. C.; Block, S. M. Optical Trapping. *Rev. Sci. Instrum.* **2004**, *75* (9), 2787–2809. https://doi.org/10.1063/1.1785844.

(11) Urban, A. S.; Carretero-Palacios, S.; Lutich, A. A.; Lohmüller, T.; Feldmann, J.; Jäckel, F.

Optical Trapping and Manipulation of Plasmonic Nanoparticles: Fundamentals, Applications, and Perspectives. *Nanoscale* **2014**, *6* (9), 4458. https://doi.org/10.1039/c3nr06617g.

(12) Svoboda, K.; Block, S. M. Optical Trapping of Metallic Rayleigh Particles. *Opt. Lett.* **1994**, *19* (13), 930–932. https://doi.org/10.1364/OL.19.000930.

(13) Skelton Spesyvtseva, S. E.; Dholakia, K. Trapping in a Material World. *ACS Photonics* **2016**, *3*, 719–736. https://doi.org/10.1021/acsphotonics.6b00023.

(14) Hansen, P. M.; Bhatia, V. K.; Harrit, N.; Oddershede, L. Expanding the Optical Trapping Range of Gold Nanoparticles. *Nano Lett.* **2005**, *5* (10), 1937–1942. https://doi.org/10.1021/nl051289r.

(15) Dienerowitz, M.; Mazilu, M.; Dholakia, K. Optical Manipulation of Nanoparticles: A Review. *J. Nanophotonics* **2008**, *2* (1), 021875. https://doi.org/10.1117/1.2992045.

(16) Rajapaksa, I.; Uenal, K.; Wickramasinghe, H. K. Image Force Microscopy of Molecular Resonance: A Microscope Principle. *Appl. Phys. Lett.* **2010**. https://doi.org/10.1063/1.3480608.

(17) Jahng, J.; Fishman, D. A.; Park, S.; Nowak, D. B.; Morrison, W. A.; Kumar Wickramasinghe, // H; Potma, E. O. Linear and Nonlinear Optical Spectroscopy at the Nanoscale with Photoinduced Force Microscopy. **2015**. https://doi.org/10.1021/acs.accounts.5b00327.

(18) Prikulis, J.; Svedberg, F.; Ka, M.; Enger, J.; Ramser, K.; Gokso, M.; Hanstorp, D. Optical Spectroscopy of Single Trapped Metal Nanoparticles in Solution. *Nano Lett.* **2004**, *4* (1), 115–118. https://doi.org/10.1021/nl0349606.

(19) Pearce, K.; Wang, F.; Reece, P. J. Dark-Field Optical Tweezers for Nanometrology of Metallic Nanoparticles. *Opt. Express* **2011**, *19* (25), 25559. https://doi.org/10.1364/oe.19.025559.

(20) Tolić-Nørrelykke, S. F.; Schäffer, E.; Howard, J.; Pavone, F. S.; Jülicher, F.; Flyvbjerg, H. Calibration of Optical Tweezers with Positional Detection in the Back Focal Plane. *Rev. Sci. Instrum.* **2006**, *77* (10). https://doi.org/10.1063/1.2356852.

(21) Lee, Y. J.; Schade, N. B.; Sun, L.; Fan, J. A.; Bae, D. R.; Mariscal, M. M.; Lee, G.; Capasso, F.; Sacanna, S.; Manoharan, V. N.; et al. Ultrasmooth, Highly Spherical Monocrystalline Gold Particles for Precision Plasmonics. *ACS Nano* **2013**, *7* (12), 11064–11070. https://doi.org/10.1021/nn404765w.

(22) Tcherniak, A.; Dominguez-Medina, S.; Chang, W. S.; Swanglap, P.; Slaughter, L. S.; Landes, C. F.; Link, S. One-Photon Plasmon Luminescence and Its Application to Correlation Spectroscopy as a Probe for Rotational and Translational Dynamics of Gold Nanorods. *J. Phys. Chem. C* **2011**, *115* (32), 15938–15949. https://doi.org/10.1021/JP206203S/SUPPL_FILE/JP206203S_SI_001.PDF.

(23) Nugent-Glandorf, L.; Perkins, T. T. Measuring 0.1-Nm Motion in 1 Ms in an Optical

Microscope with Differential Back-Focal-Plane Detection. *Opt. Lett.* **2004**, *29* (22), 2611–2613.

(24) Pesce, G.; Jones, P. H.; Maragò, O. M.; Volpe, G. Optical Tweezers: Theory and Practice. *Eur. Phys. J. Plus* **2020**, *135*, 949. https://doi.org/10.1140/EPJP/S13360-020-00843-5.

(25) Seol, Y.; Carpenter, A. E.; Perkins, T. T. Gold Nanoparticles: Enhanced Optical Trapping and Sensitivity Coupled with Significant Heating. *Opt. Lett.* **2006**, *31* (16), 2429–2431. https://doi.org/10.1364/OL.31.002429.

(26) Svoboda, K.; Block, S. M. Biological Application of Optical Forces. *Annu. Rev. Biophys. Biomol. Struct.* **1994**, *23*, 247–285.

(27) Jones, P. H.; Maragò, O. M.; Volpe, G. *Optical Tweezers: Principles and Applications*; Cambridge University Press, 2015.

(28) Pralle, A.; Prummer, M.; Florin, E.-L.; Stelzer, E. H. K.; Horber, J. K. H. Three-Dimensional High-Resolution Particle Tracking for Optical Tweezers by Forward Scattered Light. *Microsc. Res. Tech.* **1999**, *386* (November 1998), 378–386.